Cardiovasc Intervent Radiol (2009) 32:320–325
DOI 10.1007/s00270-008-9447-9

TECHNICAL NOTE

MR-Guided Laser Ablation of Osteoid Osteoma in an Open High-Field System (1.0 T)

F. Streitparth · B. Gebauer · I. Melcher · K. Schaser · C. Philipp · J. Rump · B. Hamm · U. Teichgräber

Received: 31 July 2008 / Accepted: 4 September 2008 / Published online: 4 October 2008

Abstract Computed tomography is the standard imaging modality to minimize the extent of surgical or ablative treatment in osteoid osteomas. In the last 15 years, since a description of thermal ablation of osteoid osteomas was first published, this technique has become a treatment of choice for this tumor. We report the case of a 20-year-old man with an osteoid osteoma treated with laser ablation in an open high-field magnetic resonance imaging scanner (1.0 T). The tumor, located in the right fibula, was safely and effectively ablated under online monitoring. We describe the steps of this interventional procedure and discuss related innovative guidance and monitoring features and potential benefits compared with computed tomographic guidance.

Keywords Osteoid osteoma · Laser ablation · Open MRI · MR thermometry

F. Streitparth (✉) · B. Gebauer · J. Rump · B. Hamm · U. Teichgräber
Department of Radiology, Charité, Humboldt-University, Charitéplatz 1, 10117 Berlin, Germany
e-mail: florian.streitparth@charite.de

B. Gebauer
e-mail: bernhard.gebauer@charite.de

J. Rump
e-mail: jens.rump@charite.de

B. Hamm
e-mail: bernd.hamm@charite.de

U. Teichgräber
e-mail: ulf.teichgraeber@charite.de

I. Melcher · K. Schaser
Center for Musculoskeletal Surgery, Charité, Humboldt-University, Charitéplatz 1, 10117 Berlin, Germany

I. Melcher
e-mail: ingo.melcher@charite.de

K. Schaser
e-mail: klaus-dieter.schaser@charite.de

C. Philipp
Department of Laser Medicine, Elisabeth Klinik, Berlin, Germany
e-mail: cmphilipp@web.de

Introduction

Osteoid osteoma is a benign osteoblastic tumor that usually occurs in the first three decades of life with a male predominance [1]. The typical symptom is severe local pain at the tumor site, which typically worsens at night and responds well to nonsteroidal anti-inflammatory drugs (NSAIDs). In the past, en bloc resection and curettage of the nidus have been the standard treatments, but because of difficulties in intraoperative nidus localization, the extent of surgical resection was disproportional to the nidal size [2]. Since Rosenthal et al. [3] first described computed tomography (CT)-guided thermal ablation of osteoid osteomas in 1992, this minimally invasive technique has become increasingly popular. Besides radiofrequency ablation (RFA) [3, 4], laser ablation has been successfully applied in the treatment of osteoid osteomas under CT guidance [5–10].

So far, to our knowledge, only one publication has described magnetic resonance imaging (MRI) guidance of treating this tumor; an open low-field scanner at 0.23 T was used, and thermal monitoring was not yet proven to be feasible [9]. We herein report a case of symptomatic osteoid osteoma treated by laser ablation under MRI

guidance and monitoring in an open high-field system at 1.0 T.

Case Report

A 20-year-old man sought care for severe local pain in the medial diaphysis of the right lateral fibula for 6 months, which worsened at night and typically responded to treatment with NSAIDs. X-ray and MRI were performed demonstrating pathognomonic image findings, suggesting an osteoid osteoma: a 5-mm translucent tumor nidus and surrounding reactive sclerosis of the cortical bone (Fig. 1). The patient was referred to our department for removal of the osteoid osteoma. The patient was informed at treatment of possible complications and treatment alternatives (NSAID treatment, surgery, CT-guided surgery, CT-guided drill excision, and thermoablation) by an orthopedic surgeon and an interventional radiologist. Informed consent was obtained. The study plan was accepted in the institutional ethics committee of our clinic.

We planned to use our knowledge in CT-guided radiofrequency and laser ablation in osteoid osteoma to treat the patient by laser ablation under MRI-guidance and monitoring in an open high-field MRI (1.0 T, Panorama HFO, Philips, Best, Netherlands) (Fig. 2). Apart from the MRI scanner, the open "interventional" MRI system comprises a workstation with full scanner control, an in-room monitor, a Bluetooth mouse (custom made) for operator-controlled sequence initiation, and a Flex S coil (single loop type, diameter 15 cm).

The patient received intravenous prophylactic antibiotics before the procedure (cefuroxim-ratiopharm 1.5 g, Ulm, Germany) and was operated on while under general anesthesia. Local anesthetics were applied (Xylonest 1%, AstraZeneca, Wedel, Germany) subcutaneously and periperiostically to reduce local postprocedural pain.

Interactive lesion localization, instrument guidance, drilling, and positioning of the laser fiber into the opened tumor were guided in near real-time imaging with a fast T1-w turbo spin echo (TSE) sequence (TE/TR 5.7/200 ms, TF 7, fa 90°, scan duration 3 s). A MRI-compatible 4-mm bone biopsy drill (Invivo, Schwerin, Germany) was used to enter the nidus with freehand technique (Fig. 3). An experienced pathologist analyzed the bone specimen. An 18-g coaxial needle (Somatex, Teltow, Germany) was introduced through the biopsy access channel with real-time MRI. The needle position was then verified with a PD-w TSE sequence (TE/TR 30/383 ms, TF 11, fa 90°, scan duration 41 s). A 400-µm bare laser fiber (Dornier MedTech, Wessling, Germany) was introduced through the needle. The needle was then retracted 5 mm and its position confirmed once more. Subsequent laser treatment with a Nd:YAG laser (1064 nm, Fibertom Medilas, Dornier MedTech, Wessling, Germany) was conducted with continuous energy flow and an effective output of 2.3 watts (W_{eff}). The total energy deposition to the bone tissue amounted to 1498 J in 11 min treatment time. A T1-w gradient echo (GRE) sequence (TE/TR 2/4.3 ms; fa 27°), enabling image update every 4 s, was used for online monitoring of the T1 temperature tissue effects.

Further data sets were used to calculate the quantification of temperature changes. For this purpose, a software tool based on IDL (Interactive Data Language, Research Systems Inc., Boulder, CO) was implemented on an alternate workstation. It enables the display of temperature and tissue alterations based on SI changes derived from phase images of the GRE sequence. To further enhance visualization of SI changes during laser treatment, a color-coded subtraction method was used (Fig. 4). Direct postinterventional, contrast-enhanced (Magnevist; Bayer-Schering, Berlin, Germany) MRI was performed to confirm total ablation, typically showing loss of nidal contrast enhancement (Fig. 5) [8, 11].

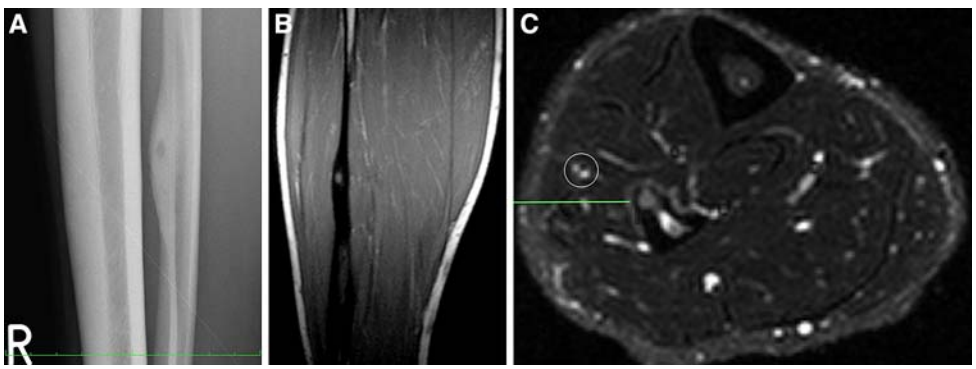

Fig. 1 A 20-year-old man with history of typical clinical symptoms and typical imaging findings suggesting osteoid osteoma with a translucent tumor nidus, 5 mm in diameter, and a surrounding reactive sclerosis of the cortical fibular bone in conventional X ray (**A**) and MRI (**B**, **C**). (**B**) T1-w TSE in parasagittal plane. (**C**) STIR in axial orientation. The line indicates the planning of puncture route to avoid lesion of the peronaei vessels (*circled*)

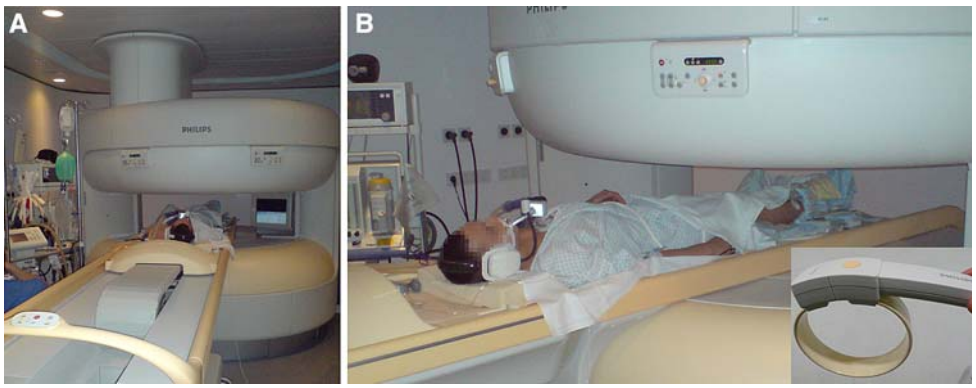

Fig. 2 (**A**) View of patient positioned in the open high-field MRI (1.0 T, Panorama HFO, Philips) for real-time MR-guided laser ablation of an osteoid osteoma of the right fibula. Needle insertion and laser release during intervention are visible on an in-room monitor beside the magnet. (**B**) Lower extremity placed in dedicated surface flex coil, which was placed over the region of interest positioned in magnet isocenter

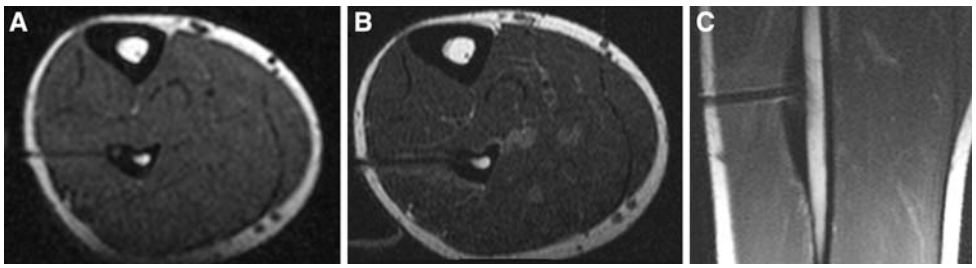

Fig. 3 Real-time MR-guided drilling of the osteoid osteoma of the right fibula with freehand technique. (**A**) T1-w TSE (TE/TR 5.7/200, acquisition time 3.0 s) shows needle tip approaching the 5-mm target lesion in the medial diaphysis of the lateral fibula. The needle trajectory is from a lateral direction to prevent lesion of the peronaei vessels, consequently yielding an excellent instrument artifact as a result of the 90° position to B0. (**B**, **C**) PD-w TSE (TE/TR 30/383, acquisition time 41 s) images verify instrument placement inside the nidus after hand drill procedure. Comparison of the real time T1-w TSE with the PD-w sequence for verification shows similarly adequate image quality in display of needle and target lesion. Note the additional benefit of multiplanar navigation in a parasagittal plane (**C**)

The operative time from starting the procedure (tumor localization) to the end of the procedure (postinterventional control) was 120 min. During the procedure, a total of 10 planning, interventional, temperature sensitive, and post-procedural imaging sequences were performed. The nidus was successfully localized, targeted, and treated under magnetic resonance (MR) fluoroscopy and thermometry. The laser effect was reliably depicted online. A signal change in MRI images of the treated area was observed during thermal ablation. The color-coded technique was found to be valuable in addition to conventional magnitude images. No complications occurred.

The patient was symptom-free after treatment. After the procedure, the patient was monitored for 6 h in the recovery room. He was discharged from the hospital 24 h after treatment. At a 3-month follow-up, the patient remains asymptomatic, without the need for oral antiphlogistics.

Discussion

Osteoid osteoma is a benign tumor in young individuals that causes pain and secondary malpositioning or scoliosis. Increased production of prostaglandins and increased vascularization in the nidus are supposed to be responsible for clinical symptoms and the quick response to NSAIDs. Standard treatment in the past was en bloc resection of the nidus, which consisted of a resection disproportional to the size of the nidus and lengthy recovery after surgery.

In a previous study, we compared laser to radiofrequency-induced ablation of osteoid osteoma and showed comparable results (primary success, recurrent pain, complication rate) for both techniques [8]. These results are in accordance with recent studies reporting thermal ablative tumor therapy in osteoid osteoma (RFA initial success 91%, recurrent pain 5%; laser 99.1% and 10.2%, respectively) [4, 7]. We assume that thermal destruction, tissue

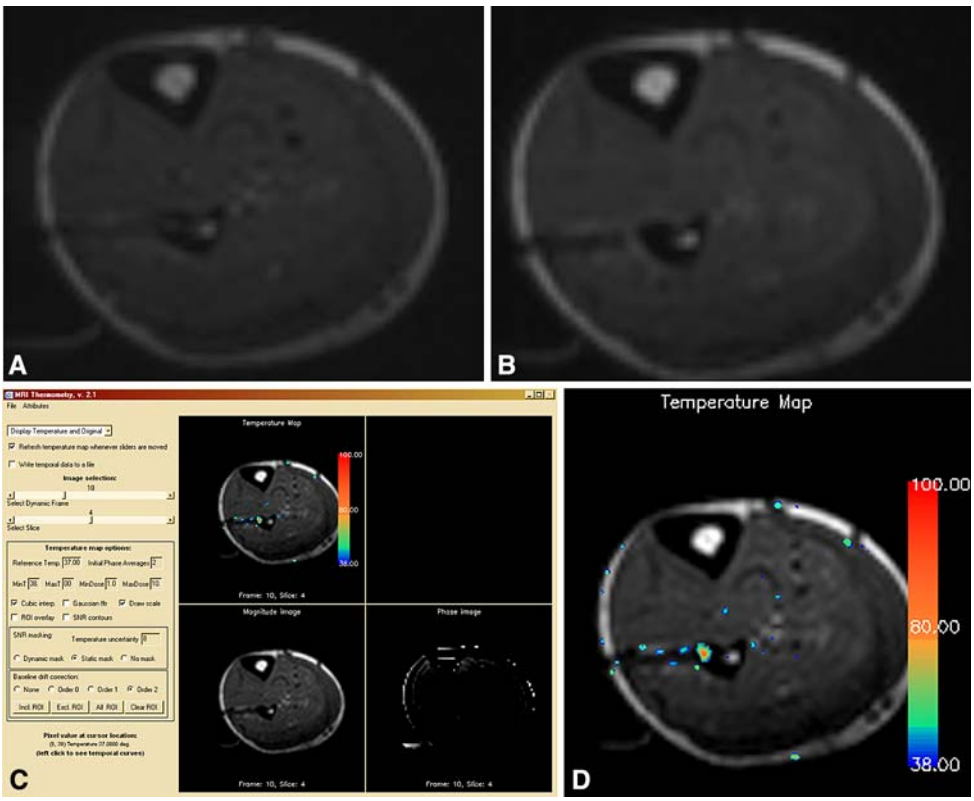

Fig. 4 MR thermometry with T1-w GRE (TE/TR 2/4.3 ms; fa 27°, acquisition time 4 s) (**A**) at the beginning of the laser ablation and (**B**) after 11 min. Note the T1 effect as a hypointensity of the ablation area, indicating qualitative temperature rating. (**C**, **D**) Display of software interface for temperature mapping demonstrating temperature and tissue alterations based on SI changes derived from phase images of the GRE sequence with a color-coded subtraction method

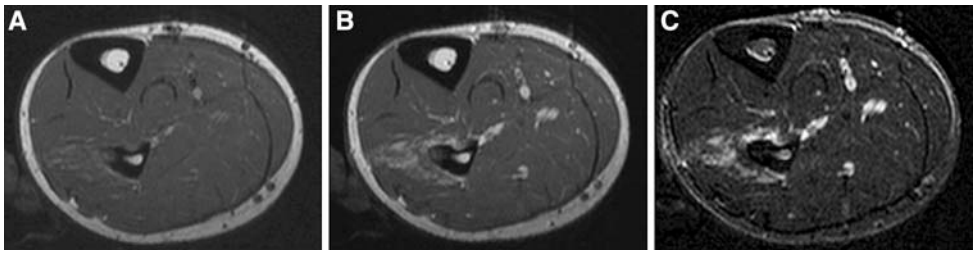

Fig. 5 Postinterventional control in the open high-field MRI. Subtraction image (**C**) of T1-w TSE native (**A**) and contrast-enhanced T1-w TSE (**B**) was performed to confirm total ablation, typically showing loss of nidal contrast enhancement (**C**)

coagulation, devascularization, and denervation are key to successful treatment by thermal ablation. The technical success is not dependent on the heating technique. However, in contrast to RFA, laser is fully MRI compatible. Hence, online MR thermometry without the need to discontinue thermal ablation is possible. We used an open high-field MRI scanner (1.0 T, Panorama HFO, Philips) (Fig. 2), which provided good patient access, high-quality imaging for lesion localization (Fig. 1) and instrument guidance (Fig. 3), online temperature monitoring during treatment (Fig. 4), and postprocedural imaging to rule out missed nidal areas (Fig. 5), resulting in a "one-stop-shop" intervention.

CT has a high spatial resolution for calcified bone structures and also enables real-time fluoroscopy, which makes percutaneous interventions straightforward. MRI, however, has features that are potentially advantageous when compared with CT in image-guided microtherapy. Even in interactive sequences, MRI permits superior soft tissue resolution. Thus, MRI enables reliable detection of critical soft tissue structures (nerves, vessels), which is of primary importance when performing bone interventions. CT provides equivalent information with inferior contrast and the occasional necessity of administering contrast agent. The osteoid osteoma nidus can be reliably identified and targeted with MRI. Interactive MRI allows for split-second image updates. Further, the capability of multiplanar pre- and intraprocedural MRI provides the interventionalist with essential information. The instrument-induced artifact sizes, which vary according to the field strength, instrument position to B0, and instrument-inherent susceptibility qualities [12], must be taken into account when planning the procedure. By means of passive needle tracking, the artifact of the needle typically overestimates the true needle size. This problem may limit the safety of the procedure, particularly in critical regions, e.g.,

close to the joint, in vertebral lesions, or in the small bones of the hands and feet [13]. In these regions CT mostly provides a better depiction of the anatomy and thus more precise needle placement. The interactive TSE sequence that we used imaged the instrument's actual location and size as realistically as possible; in a high magnetic field setting, TSE is more practical than GRE because TSE produces a better delineated artifact. The in-room Bluetooth mouse for operator-controlled sequence initiation and switch in multiplanar navigation facilitated real-time controlling of instrument position and thus increased speed and accuracy of the intervention.

Regarding online monitoring of the temperature spread within the tissue, other authors have reported on similar strategies in low-field open MRI (0.23 T) [9], which, however, have not been approved. Generally, high-field devices are more suitable for thermal monitoring as a result of an improved signal-to-noise ratio. With the use of the open high-field scanner at 1.0 T, we can now provide improved high-quality imaging with increased resolution. In our preclinical ex vivo investigations as well as in this clinical case, we could image a signal change of the treated area during laser ablation with a fast GRE sequence. Thus, we qualitatively detected the change in T1 relaxation time and related signal void caused by increasing temperature within the tissue [14]. Because the T1 effect does not correlate linearly with the increase of temperature, we have further shown the feasibility of temperature calculation with phase images and a color-coded subtraction technique indicating quantitative thermometry [15]. Reliability of temperature measurement depends on the presence of needle artifacts. The GRE sequence used has a short echo time (TE) and proved appropriate in monitoring thermal tissue changes at the needle tip. A short TE was chosen because the needle artifact increases with longer TE. The reliability to quantitatively monitor thermal changes in bone has to be proven in further investigations comprising larger number of patients.

Whether or not postinterventional contrast-enhanced MRI can detect incomplete nidal ablation is under current investigation in our patient population treated by CT-guided RFA ($n = 50$). In a recent study, MRI demonstrated a characteristic appearance and subsequent changes of RFA-treated areas for osteoid osteoma during follow-up [11]. Potentially, the direct postinterventional control within the presented "one-stop-shop" procedure could be crucial in avoiding recurrences.

In our case, the biopsy result was nonspecific fibrosis without definitive nidus in histology. Although the diagnosis was not completely conclusive, the patient was free of symptoms 3 months after treatment.

Progress in imaging techniques has greatly facilitated the treatment of osteoid osteomas, allowing excellent outcome with limited morbidity. Particularly regarding osteoid osteomas in more difficult, nondiaphyseal localizations, current strategies such as the MRI guidance and monitoring in an open high-field scanner may be of significance for effective and safe treatment. The costs of MRI-guided laser ablation in a previous publication were lower than the costs of either superficial or deep excision [16], and the costs of the described MRI-guided laser ablation are comparable to the costs of CT-guided RFA within our institution. Although the costs depend on time and scanner type (MR is more expensive than CT), this is the result of the lower cost of the laser bare fiber (which can be autoclaved; cost, approximately €200) in relation to the RFA applicator (single use; cost, approximately €800). Although a 20 W laser costs €20,000 and is more expensive compared with a radiofrequency generator, a Nd:YAG or diode laser is usually available in medium to large hospitals, since these lasers are also used by specialists in other disciplines [7].

In relation to CT guidance, the avoidance of ionizing radiation in MRI for the young adult and the interventionalist is another main point.

In conclusion, MRI guidance and thermal monitoring of percutaneous laser ablation of osteoid osteoma is feasible within open 1.0 T systems for a "one-stop-shop" intervention. This minimally invasive treatment with rapid image updates with fast TSE and GRE sequence designs describes one step on the way to a safer procedure.

Acknowledgments We thank Virginia Ding-Reinelt, MRI technician, and Heidi Kotalla, surgical nurse, for their collaboration and support.

References

1. Kransdorf MJ, Stull MA, Gilkey FW, Moser RP Jr (1991) Osteoid osteoma. Radiographics 11:671–696
2. Sluga M, Windhager R, Pfeiffer M et al (2002) Peripheral osteoid osteoma. Is there still a place for traditional surgery? J Bone Joint Surg Br 84:249–251
3. Rosenthal DI, Alexander A, Rosenberg AE, Springfield D (1992) Ablation of osteoid osteomas with a percutaneously placed electrode: a new procedure. Radiology 183:29–33
4. Rosenthal DI, Hornicek FJ, Torriani M et al (2003) Osteoid osteoma: percutaneous treatment with radiofrequency energy. Radiology 229:171–175
5. Cool P, Williams DH, Pullicino V (2001) Interstitial laser photocoagulation for the treatment of osteoid osteoma. J Bone Joint Surg Br 83:462
6. DeFriend DE, Smith SP, Hughes PM (2003) Percutaneous laser photocoagulation of osteoid osteomas under CT guidance. Clin Radiol 58:222
7. Gangi A, Alizadeh H, Wong L et al (2007) Osteoid osteoma: percutaneous laser ablation and follow-up in 114 patients. Radiology 242:293
8. Gebauer B, Tunn PU, Gaffke G et al (2006) Osteoid osteoma: experience with laser- and radiofrequency-induced ablation. Cardiovasc Intervent Radiol 29:210

9. Sequeiros RB, Hyvonen P, Sequeiros AB et al (2003) MR imaging-guided laser ablation of osteoid osteomas with use of optical instrument guidance at 0.23 T. Eur Radiol 13:2309
10. Witt JD, Hall-Craggs MA, Ripley P et al (2000) Interstitial laser photocoagulation for the treatment of osteoid osteoma. J Bone Joint Surg Br 82:1125
11. Lee MH, Ahn JM, Chung HW et al (2007) Osteoid osteoma treated with percutaneous radiofrequency ablation: MR imaging follow-up. Eur J Radiol 64:309–314
12. Butts K, Pauly JM, Daniel BL et al (1999) Management of biopsy needle artifacts: techniques for RF-refocused MRI. J Magn Reson Imaging 9:586–595
13. Zouari L, Bousson V, Hamze B et al (2008) CT-guided percutaneous laser photocoagulation of osteoid osteomas of the hands and feet. Eur Radiol (in press)
14. Germain D, Vahala E, Ehnholm GJ et al (2002) MR temperature measurement in liver tissue at 0.23 T with a steady-state free precession sequence. Magn Reson Med 47:940–947
15. Rieke V, Butts Pauly K (2008) MR thermometry. J Magn Reson Imaging 27:376–390
16. Ronkainen J, Blanco SR, Tervonen O (2006) Cost comparison of low-field (0.23 T) MRI-guided laser ablation and surgery in the treatment of osteoid osteoma. Eur Radiol 16:2858